Superconducting quantum interference device with frequency-dependent damping: Readout of flux qubits

T. L. Robertson,[1] B. L. T. Plourde,[1,*] T. Hime,[1] S. Linzen,[1,†] P. A. Reichardt,[1] F. K. Wilhelm,[2] and John Clarke[1]

[1]*Department of Physics, University of California, Berkeley, California 94720-7300, USA*
[2]*Physics Department, Arnold Sommerfeld Center for Theoretical Physics and Center for NanoScience,
Ludwig-Maximilians-Universität München, 80333 München, Germany*

Recent experiments on superconducting flux qubits, consisting of a superconducting loop interrupted by Josephson junctions, have demonstrated quantum coherence between two different quantum states. The state of the qubit is measured with a superconducting quantum interference device (SQUID). Such measurements require the SQUID to have high resolution while exerting minimal backaction on the qubit. By designing shunts across the SQUID junctions appropriately, one can improve the measurement resolution without increasing the backaction significantly. Using a path-integral approach to analyze the Caldeira-Leggett model, we calculate the narrowing of the distribution of the switching events from the zero-voltage state of the SQUID for arbitrary shunt admittances, focusing on shunts consisting of a capacitance C_s and resistance R_s in series. To test this model, we fabricated a dc SQUID in which each junction is shunted with a thin-film interdigitated capacitor in series with a resistor, and measured the switching distribution as a function of temperature and applied magnetic flux. After accounting for the damping due to the SQUID leads, we found good agreement between the measured escape rates and the predictions of our model. We analyze the backaction of a shunted symmetric SQUID on a flux qubit. For the given parameters of our SQUID and realistic parameters for a flux qubit, at the degeneracy point we find a relaxation time of 113 μs, which limits the decoherence time to 226 μs. Based on our analysis of the escape process, we determine that a SQUID with purely capacitive shunts should have narrow switching distributions and no dissipation.

I. INTRODUCTION

Superconducting devices are attractive candidates for quantum bits (qubits) because of their manufacturability, controllability, and scalability. As with any qubit, strong interaction is necessary to control its state and to measure the outcome of a computation; however, the quantum properties are very fragile and only become manifest in almost total isolation. Reconciling these contradictory requirements is the fundamental challenge in building a quantum computer.

Quantum coherent behavior has been demonstrated in devices based on the flux in a superconducting ring interrupted by Josephson junctions.[1–6] With an applied flux bias of $\Phi_0/2$, where $\Phi_0 \equiv h/2e$ is the flux quantum, the qubit has two degenerate states corresponding to its screening flux being oriented parallel or antiparallel to the applied flux. The detector used to measure the qubit must have sufficient sensitivity to distinguish between the two states of the qubit efficiently, but must not cause excessive decoherence during the quantum evolution of the system. A conventional, resistively shunted dc superconducting quantum interference device (SQUID) is an excellent linear flux detector with high sensitivity when operated in a flux-locked loop,[7] but noise currents generated by the shunt resistors induce qubit decoherence, rendering it unsuitable.

Because the qubit is only a two-state system, a linear detector provides more information than necessary. An unshunted SQUID is widely used as a flux comparator[1] to distinguish the two states of the qubit, and furthermore has negligible dissipation in the superconducting state, making it an attractive candidate for a qubit meter. For a given bias current, one value of flux causes the SQUID to switch, generating an easily detectable voltage, while for another flux the SQUID remains in the supercurrent state. By properly engineering the appropriate parameters, one can use this device to discriminate between the two states of the qubit.

While the unshunted SQUID has minimal inherent dissipation, the leads coupling it to external measurement electronics can drive noise currents around the loop, causing decoherence in the qubit, particularly if the SQUID has typical fabrication asymmetries.[8] This decoherence can be mitigated by reducing the mutual inductance between the SQUID and the qubit; however, the concomitant reduction in the qubit signal coupled to the SQUID makes it important to optimize its resolution.

The switching of the SQUID out of the zero-voltage state is not necessarily sharp. Switching occurs when the phase particle representing the state of the SQUID escapes from the effective tilted washboard potential; the distribution of switching probabilities is governed by thermal activation over and quantum tunneling through a barrier. At high temperatures, the thermal escape rate dominates and the distribution narrows as the temperature is lowered; however, below a crossover temperature T^*, the quantum rate dominates and the distribution width is constant with decreasing temperature, limiting the resolution of unshunted SQUIDs at low temperature. The crossover temperature T^* is determined by the plasma frequency of the SQUID.[9] Appropriately engineered shunts in parallel with the SQUID junctions can renormalize the plasma frequency, depressing the crossover
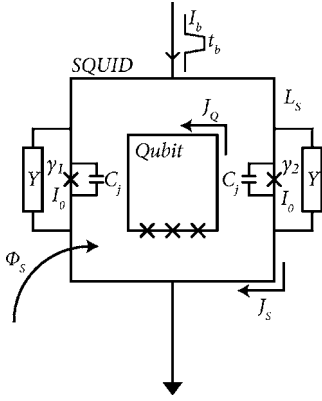
FIG. 1. Schematic of flux qubit coupled to readout SQUID.

temperature, and leading to narrower switching distribution widths and improved SQUID resolution at low temperatures. Indeed, in an early experiment that provided spectroscopic evidence for quantum coherence in a flux qubit[1] the authors placed a discrete capacitor across their SQUID.

In this paper we consider the escape from the supercurrent state of a dc SQUID with arbitrary shunts across the junctions, with emphasis on a shunt that consists of a resistor R_s in series with a capacitor C_s. In Sec. II, we calculate the switching current distribution widths for such a device, and in Sec. III fit this model to the measured escape width as a function of temperature for an experimental device. In Sec. IV, we treat the problem of decoherence of a flux qubit coupled to an arbitrarily shunted SQUID using the spin-boson model. Using the parameters for the experimental RC-shunted SQUID as a case study, we describe a set of qubit parameters which lead to very low relaxation and dephasing rates for the qubit due to the RC shunts, while allowing single-shot resolution of the qubit state. In Sec. V we conclude that a SQUID with purely capacitive shunts provides the ideal combination of narrow switching distributions without contributing additional decoherence.

II. CALCULATIONS OF ESCAPE RATES

We consider a flux qubit coupled to a dc SQUID with a mutual inductance M_{QS}, shown in Fig. 1. The SQUID consists of a superconducting loop of inductance L_S containing two Josephson junctions, each with thermodynamic critical current I_0, capacitance C_j, and shunt admittance Y. The dynamics of the SQUID are described by the phase differences across the junctions $\gamma_{1,2}$.[10] Leads attached to the SQUID loop can be used to drive a bias current I_b through the SQUID and to measure the voltage across it. The SQUID is biased with an externally applied flux $\Phi_S = \Phi_0 \phi_S / 2\pi$, and the qubit couples an additional flux $\Delta\Phi_Q = \pm M_{QS} J_Q$ depending on the sense of its circulating current J_Q. A variation in the total flux coupled to the SQUID changes the circulating current J_S flowing around the SQUID loop and the value of I_b at which the SQUID has a probability p of switching out of the zero-voltage state, $I_s^{(p)}$. This flux response $I_s^{50\%}(\Phi_S)/2I_0$ is governed by the screening parameter $\beta_L = 2L_S I_0 / \Phi_0$. A square pulse of bias current, with height I_b and duration t_b,
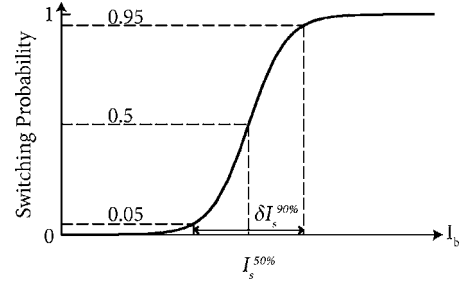
causes the SQUID to switch with a probability depending on these parameters, the qubit state and temperature. Our goal is to design a SQUID and shunts so that we can distinguish the two states of the qubit in a single shot, with well characterized and small backaction from the SQUID to the qubit. Single shot implies that when the qubit is in one state, a particular value of I_b causes the SQUID to switch with a small probability, while when the qubit is in the other state, the same I_b causes the SQUID to switch with a probability approaching unity.

A useful metric for characterizing the sensitivity of a particular SQUID readout scheme is the resolution ρ which we can express in terms of the switching distribution width δI_s and the slope of the flux modulation curve $dI_s^{50\%}/d\Phi_S$ through the equation

$$\rho^{(\Delta p)} \equiv \delta I_s^{(\Delta p)} / |dI_s^{50\%}/d\Phi_S|. \tag{1}$$

Here, Δp is a parameter that indicates how much of the switching distribution is to be included (Fig. 2). Thus, the criterion for single-shot readout with a confidence level of Δp is $\rho^{(\Delta p)} \leqslant 2\Delta\Phi_Q$.

Equation (1) shows that the resolution of a readout SQUID can be improved either by increasing $|dI_s^{50\%}/d\Phi_S|$ or by narrowing $\delta I_s^{(\Delta p)}$. The flux modulation characteristics, which are determined by the critical current and loop inductance, are often constrained by considerations related to the qubit. In particular, designing a readout SQUID which can also function as a controllable qubit coupler leads to the regime $\beta_L \ll 1$.[11] In this paper we focus on optimizing ρ by minimizing $\delta I_s^{(\Delta p)}$.

The switching distribution width of the readout SQUID is determined by two stochastic processes, thermal activation and quantum tunneling. Switching from the supercurrent to the voltage state occurs when the phase particle, representing the state of the SQUID, escapes from a metastable local minimum of the potential energy to a running state. In the thermal regime, the rate at which the SQUID switches is given by the Arrhenius expression[12]

$$\Gamma_{\text{th}}(T) = (\omega_r / 2\pi)\exp(-U_0 / k_B T), \tag{2}$$

where ω_r is the frequency of small oscillation aligned with the direction of escape, renormalized by coupling to environmental degrees of freedom, and U_0 is the height of the barrier blocking escape.

FIG. 2. Idealized SQUID switching distribution. As I_b is increased, the probability of the SQUID switching increases from 0 to 1 over a characteristic width $\delta I_s^{(\Delta p)}$.

An intuitive model of this escape process is provided by the one-dimensional dynamics of a single, undamped Josephson junction with critical current $\hat{I}_0$ and capacitance $\hat{C}_j$. In this case, for $I_b \sim \hat{I}_0$, we can write closed form approximations for the barrier height $\hat{U}_0$ and the frequency of small oscillation $\hat{\omega}_0$ as[13]

$$\hat{U}_0 \approx (4\sqrt{2}\hat{I}_0\Phi_0/6\pi)(1 - I_b/\hat{I}_0)^{3/2} \qquad (3)$$

and

$$\hat{\omega}_0 \approx \sqrt{2\pi\hat{I}_0/\Phi_0\hat{C}_j}(1 - I_b^2/\hat{I}_0^2)^{1/4}. \qquad (4)$$

We rewrite Eqs. (2) and (3) in the scaling form

$$\hat{\Gamma}_{th}(T) = \frac{\hat{\omega}_0}{2\pi}\exp-\left[\left(1 - \frac{I_b}{\hat{I}_0}\right)\left(\frac{\hat{U}_0}{k_BT}\right)^{2/3}\right]^{3/2}, \qquad (5)$$

to see that the distribution width in I_b scales as $T^{2/3}$.

In the thermal regime, the switching distributions narrow with decreasing temperature so that if the readout SQUID remained in this regime one could resolve arbitrarily small fluxes by cooling to sufficiently low temperatures. However, as the thermal fluctuations diminish, they leave behind quantum fluctuations which cause the junction to switch through tunneling and saturate the switching width to a limiting value at low temperatures. Below T^*, the switching rate saturates towards the constant value

$$\Gamma_q = \Gamma_{th}(T^*) = (\omega_r/2\pi)\exp(-U_0/k_BT^*), \quad T < T^*. \qquad (6)$$

Thus, the problem of making a sensitive readout SQUID can be recast as one of suppressing the crossover temperature, given by[12]

$$T^* = \hbar\omega_r/2\pi k_B. \qquad (7)$$

For a SQUID with given β_L, ρ is determined at low temperatures by T^*, and hence by ω_r. As we shall see, ω_r can be engineered with a properly designed shunt. Previous experiments have measured the crossover temperature for unshunted dc SQUIDs.[14,15]

We now calculate the crossover temperature for a SQUID with arbitrary loop inductance, critical current, shunt admittance, flux bias, and current bias. We use the appropriate nonohmic Caldeira-Leggett model, which contains terms renormalizing the capacitance as well as dissipative terms, and solve for the escape rates using the path-integral representation of the imaginary part of the free energy. We apply this formalism to a single, shunted Josephson junction to find an analytical formula for T^* that depends on the shunt, the plasma frequency, and the barrier height. We numerically extract these parameters from the full SQUID potential, which we shall see gives good agreement with experimental data. Thus, we reduce the SQUID with each junction shunted by an admittance Y to a single junction shunted by an effective admittance $\hat{Y} = 2Y$ (Fig. 3). The equivalent junction has a capacitance $\hat{C}_j = 2C_j$, a critical current $\hat{I}_0$ which depends on Φ_S with a maximum value $2I_0$, and a bare plasma frequency $\hat{\omega}_0$ that is derived from the SQUID plasma frequency $\omega_0(\Phi_S, I_b, \beta_L)$. This approximation neglects the SQUID loop
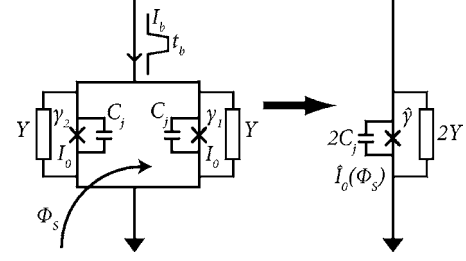
FIG. 3. Transformation from SQUID with shunt admittances Y to equivalent single Josephson junction.

inductance L_S, but is valid because the Josephson inductance of the junctions diverges near the escape point.

To compute the escape rates from Eqs. (2) and (6) for a SQUID with arbitrary β_L and Φ_S, we need to consider the full two-dimensional potential energy surface for the dc SQUID. We replace the single junction quantities $\hat{U}_0$ and $\hat{\omega}_0$ with those calculated from the full SQUID potential, U_0 and ω_0, which we use to treat the escape process in one dimension along a cut through the full SQUID potential.

The junction potential energy $\hat{U}$ is replaced with the SQUID potential energy $U = U_J + U_L$, where

$$U_L = (L_S/4)\{[(I_b/2) - J_S]^2 + [(I_b/2) + J_S]^2\} \qquad (8)$$

is the inductive energy, and

$$U_J = -\frac{\Phi_0}{2\pi}\left[I_0(\cos\gamma_1 + \cos\gamma_2) + I_b\frac{\gamma_1 + \gamma_2}{2}\right] \qquad (9)$$

is the Josephson energy. Here, J_S and $\gamma_{1,2}$ are connected through the fluxoid condition

$$\gamma_1 - \gamma_2 = 2\pi L_S J_S/\Phi_0 + \phi_S. \qquad (10)$$

The observable static solutions of this potential correspond to metastable minima along the valley of minimum U_L at points $\mathbf{x_i}$. The junction switches to the voltage state when the state of the system moves from $\mathbf{x_0}$ to $\mathbf{x_1}$ through a barrier of height U_0 at the saddle point $\mathbf{x_{01}}$ between the two minima. From this we see that $U_0 = U(\mathbf{x_{01}}) - U(\mathbf{x_0})$, and that ω_0 is related to the curvature of U at $\mathbf{x_0}$.

To find $\mathbf{x_0}$ and $\mathbf{x_{01}}$ we use previously derived analytical approximations[10] as starting points for exact numerical solutions. First, we find the critical point $\mathbf{x_c}$ where the saddle point disappears by solving the system of three equations

$$\frac{\partial U}{\partial \gamma_1} = \frac{\partial U}{\partial \gamma_2} = \frac{\partial^2 U}{\partial \gamma_1^2}\frac{\partial^2 U}{\partial \gamma_2^2} - \left(\frac{\partial^2 U}{\partial \gamma_1 \partial \gamma_2}\right)^2 = 0 \qquad (11)$$

in three unknown parameters γ_1, γ_2, and I_b. We then use the third-order expressions given in Eqs. (12) and (13) of Ref. 10 to find starting points sufficiently close to the location of the true minimum and saddle point, so that numerical methods converge. This allows us to find U_0 and ω_0 with an efficient, automated procedure. The results are displayed graphically in Fig. 4.

We derive the effective Lagrangian[16] using a method pioneered by Leggett based upon the classical equation of motion. Current conservation for the single junction can be ex-
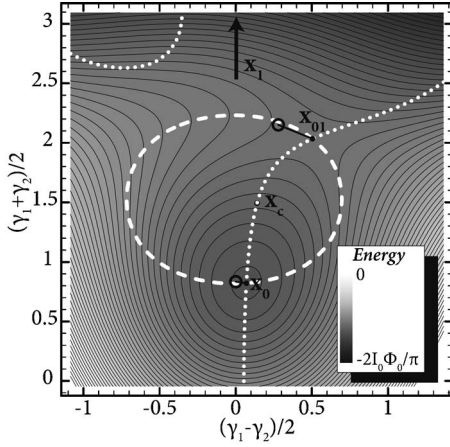
FIG. 4. SQUID potential energy. Contour plot showing the critical point $\mathbf{x_c}$, the minimum $\mathbf{x_0}$ and the saddle point $\mathbf{x_{01}}$. Open circles show the starting point for search taken from analytic approximations. White broken lines show contours where $\partial U/\partial(\gamma_1-\gamma_2)=0$ (dotted) and $\partial U/\partial(\gamma_1+\gamma_2)=0$ (dashed). SQUID parameters are: $\Phi_S=0.05\ \Phi_0$, $I_0=1.96\ \mu$A, $I_b=1.49\ \mu$A, and $L_S=500$ pH, corresponding to $\beta_L=0.95$.

pressed in terms of the inverse Fourier transform $\mathcal{F}^{-1}$ of the effective shunt admittance $\hat{Y}(\omega)$ as

$$I_b = \hat{I}_0 \sin \hat{\gamma} + \mathcal{F}^{-1}\{(\Phi_0/2\pi)i\omega\hat{\gamma}[\hat{Y}(\omega) + 2i\omega C_j]\}, \quad (12)$$

where $\hat{\gamma}$ is the phase difference across the junction. The Fourier transform of this equation yields

$$K(\omega)\hat{\gamma} = -\mathcal{F}(\partial\hat{U}/\partial\hat{\gamma}), \quad (13)$$

where $\hat{U}=(\Phi_0/2\pi)\ (I_b\hat{\gamma}-\hat{I}_0\cos\hat{\gamma})$ is the single junction potential and

$$K(\omega) = (\Phi_0/2\pi)i\omega[\hat{Y}(\omega) + 2i\omega C_j] \quad (14)$$

is the frequency-dependent linear dynamical operator.[16]

To determine the tunneling rate using the free energy method, we need to find the effective action of the system in imaginary time τ. At finite temperature, the partition function is a path integral over all periodic paths $q(\tau)$ with $q(ih/k_BT)=q(0)$. We Fourier expand these paths as $q(\tau)=\Sigma_n q(\omega_n)\exp(-i\omega_n\tau)$, where $\omega_n=2\pi nk_BT/h$ are the Bose-Matsubara frequencies, to find the effective action

$$S_{\text{eff}}[q(\omega)] = (1/2\pi)\sum_n K(-i|\omega_n|)|q(\omega_n)|^2 + S_U. \quad (15)$$

Here, S_U is the contribution of the potential energy and the analytically continued dynamical operator is given by $\bar{K}(\omega) \equiv K(-i|\omega|)$.

If the barrier is not too low, it is sufficient to evaluate the contributions to the partition function around the classical solutions: the periodic paths which make S_{eff} stationary. The escape can be driven by thermal or quantum fluctuations. These mechanisms can be distinguished by two classes of stationary solutions: thermal escape corresponds to constant paths, $q(\omega)=0$ for $\omega \neq 0$; quantum tunneling corresponds to

nontrivial periodic paths (instantons). The highest temperature with an instanton solution is T^*.

The instanton appears as a small-amplitude oscillation around the minimum of the inverted potential described by

$$\bar{K}(\omega_r) - 2C_j\hat{\omega}_0^2 = 0. \quad (16)$$

This equation for ω_r yields T^* through Eq. (7).

III. EXPERIMENTAL RESULTS

To design a SQUID to measure a flux qubit, one wants to minimize ρ while exerting a weak backaction on the qubit due to the shunts. One choice for a shunt which satisfies this compromise is an admittance Y (Fig. 1) which consists of a capacitor C_s in series with a resistor R_s. The relevant frequency for the SQUID damping is the plasma frequency $\hat{\omega}_0$ of the equivalent single junction.[17] We design the SQUID and qubit so that $\hat{\omega}_0/2\pi$ is more than an order of magnitude greater than the qubit level splitting frequency ν. We choose R_s and C_s such that $1/2\pi R_sC_s$ is larger than ν. At $\hat{\omega}_0/2\pi$, the capacitor has a negligible reactance and the resistor damps the SQUID; in contrast, at ν the shunt capacitor has an impedance greater than that of free space.

We fabricated an RC-shunted SQUID with Al-AlO$_x$-Al tunnel junctions on an oxidized Si substrate using electron-beam lithography and double-angle evaporation (Fig. 5). The junction areas were 350×260 nm^2, corresponding to a capacitance $C_j=9.3$ fF determined from separate measurements on similar junctions. The shunt capacitors were deposited in the same Al-AlO$_x$-Al layer as the tunnel junctions in an interdigitated style, with $0.6\ \mu$m wide fingers spaced by $0.8\ \mu$m. We estimate each capacitor to have a value $C_s=20$ fF, using the simple design rule that when the gap is equal to the width, and larger than the oxide thickness, the capacitance of interdigitated capacitors fabricated on silicon wafers is C (fF) $\approx 0.1 \times N \times L$ (μm), where N is the number of fingers in each electrode, and L is the length of each finger.[18,19] The shunt resistors were patterned in a 42 nm thick AuCu film to yield $R_s=40\ \Omega$, based on the measured resistor area and separate measurements of the sheet resistance. The device was cooled in a dilution refrigerator with all electrical leads to the sample heavily filtered at several different temperatures with a combination of lumped circuit and copper powder low-pass filters.[13] The sample was enclosed in a Pb-plated cavity to eliminate external magnetic field fluctuations.

Measurements of $I_s^{50\%}$ were made by adjusting the amplitude of a 4 μs long trapezoidal bias current pulse until the voltage state was detected 50% of the time out of 5000 averages. The flux applied to the SQUID was varied to produce the modulation curve shown in Fig. 6(a). By fitting the shape of the flux modulation curve to calculations based on the SQUID potential we estimated $\beta_L=0.95$; with the computed value $L_S=500$ pH we find $I_0=1.96\ \mu$A. The rise in $I_s^{50\%}$ near $\Phi_S=\pm\Phi_0/2$ is due to the switching from the L_SC_j-resonance of the SQUID, which produces a step in the current-voltage characteristic of the SQUID. This step modulates with flux with period Φ_0, $\Phi_0/2$ out of phase with the modulation of $I_s^{50\%}$.[20]
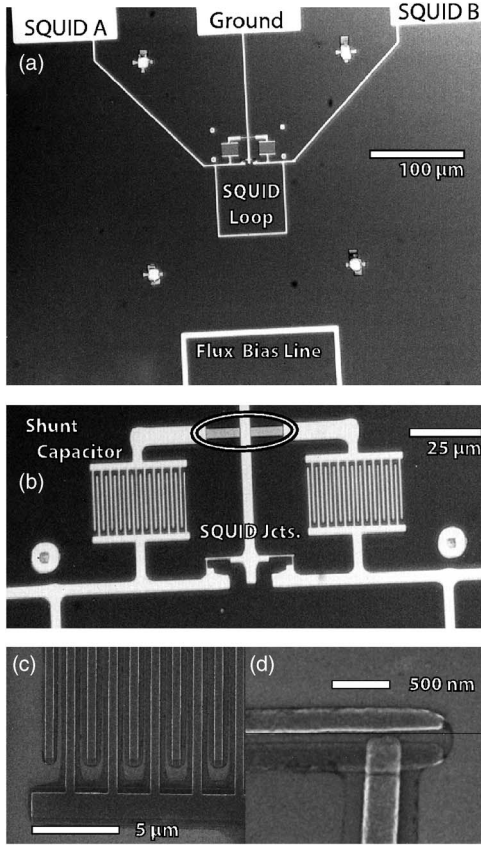
FIG. 5. Micrographs of RC-SQUID. (a) Overview showing flux bias line; leads and pads for applying bias current and detecting voltage are labeled at top. The pulse current is split symmetrically between pads "SQUID A" and "SQUID B" so that fluxes generated by this current do not couple to the qubit. (b) Enlarged view showing Josephson junctions, interdigitated capacitors, and AuCu resistors, indicated by the ellipse. (c) Capacitor detail. (d) Junction detail.

By successively measuring the switching probability as a function of the amplitude of the applied bias current pulse we acquired the curve shown schematically in Fig. 2 to determine $\delta I_s^{90\%}$ versus Φ_S [Fig. 6(b)]. From these measurements, we compute the resolution $\rho^{90\%}$ as a function of Φ_S. The results [Fig. 6(c)] show that the resolution is roughly constant at $15 m\Phi_0$ for $\Delta p = 90\%$ and $28 m\Phi_0$ for $\Delta p = 99\%$ over a range $0.2\Phi_0 < |\Phi_S| < 0.4\Phi_0$, with the resolution degenerating near $\Phi_S = n\Phi_0/2$ (n is an integer).

We measured $\delta I_s^{90\%}$ for several values of Φ_S at temperatures between 24 and 500 mK, as shown in Fig. 7. The width remains constant below $T \sim 200$ mK, indicating the quantum tunneling regime, and increases as a power law in the thermal regime. The fractional width increases as the flux bias moves away from $n\Phi_0$.

To determine the effect of the RC-shunt, we compare these data to the model described in Sec. II. A nuance in this calculation is that, because T^* depends on the plasma frequency, which in turn is a function of the bias current, one must solve self-consistently for the escape point at T^*.

For a SQUID with each junction shunted by R_s and C_s in series, the effective shunt admittance across the equivalent single Josephson junction (Fig. 3) is
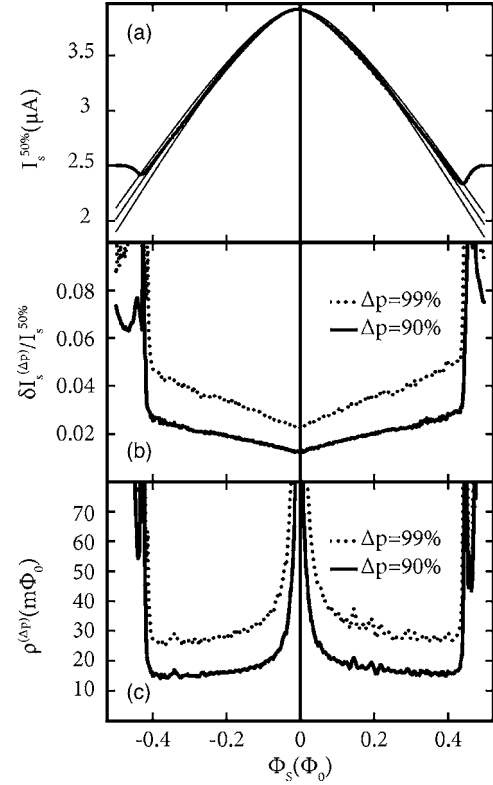
FIG. 6. (a) $I_s^{50\%}$ vs Φ_S for an RC-shunted SQUID. Thick line shows data, thin lines show calculated modulation curves for $\beta_L = 1.05$ (top), $\beta_L = 0.95$ (middle), and $\beta_L = 0.86$ (bottom). (b) Switching width $\delta I_s^{(\Delta p)}p/I_s^{50\%}$ vs Φ_S. (c) Resolution $\rho^{(\Delta p)}$ vs Φ_S. Measurements made at 24 mK.

$$\hat{Y}(\omega) = 2\omega C_s \omega_c/(\omega - i\omega_c), \qquad (17)$$

where $\omega_c = 1/R_s C_s$. Using Eq. (13) and applying the linear response formalism as described by Leggett,[16] we find that ω_r is the real root of the cubic equation

$$\omega_r^3 + \omega_c(1 + \kappa)\omega_r^2 - \omega_0^2\omega_r - \omega_c\omega_0^2 = 0, \qquad (18)$$

where $\kappa \equiv C_s/C_j$. This root can be found in closed form using Cardano's formula.[21] The parametric dependence of T^* is shown in Fig. 8. We can identify a number of limits:

(1) Very small rolloff frequency, $\omega_c \to 0$: $\omega_r = \omega_0$. This recovers the result for an unshunted junction.

(2) Small rolloff frequency, $\omega_c \to 0$, $\kappa\omega_c$ arbitrary (corresponds to the rolloff frequency with the junction capacitance of appreciable size): $\omega_r = \kappa\omega_c\{[1 + (2\omega_0/\kappa\omega_c)^2]^{1/2} - 1\}/2$. This describes a light particle with damping.

(3) High rolloff frequency, $\omega_c \gg \omega_0$: $\omega_r = \omega_0/(\kappa+1)^{1/2}$. The capacitor renormalizes the plasma frequency of the junction.

For a set of RC-shunted SQUIDs with fixed C_s and variable R_s, the first limit corresponds to $R_s \to \infty$, so that the shunt has no effect on the system. As R_s is decreased, the enhanced damping suppresses T^*. As R_s is further decreased, the dominant effect is that the shunt capacitance renormalizes the plasma frequency, suppressing T^* by a factor asymptotically
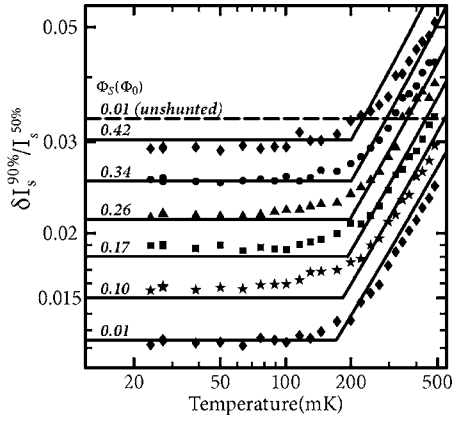
FIG. 7. Measured 90% switching width vs temperature for several different Φ_S. Solid lines show the predicted distribution widths for RC-shunted SQUID with $R_s = 40\ \Omega$, $C_j = 9.3$ fF, $I_0 = 1.96\ \mu$A, $C_s = 20$ fF, and a fit value $R_l = 52\ \Omega$. Dashed line shows calculated width for corresponding unshunted SQUID with $R_l = \infty$ at $\Phi_S = 0.01\Phi_0$.

approaching $(1 + \kappa)^{-1/2}$. Thus, one can reduce T^* by either decreasing R_s, increasing C_s, or both.

Using the parameters for our RC-shunted SQUID, we obtain escape widths that are much larger than our measured values. By treating the shunt capacitance C_s as a free parameter while keeping the rest of the device parameters unchanged, we find good agreement between theory and experiment with $C_s = 153$ fF, which yields $T^* = 171$ mK at $\Phi_S = 0.01\Phi_0$. However, this value of C_s, which we shall refer to as case A, is a factor of 8 greater than the estimated value of 20 fF. In fact, we believe that a major contribution to the narrow escape widths is the shunt admittance $1/R_l$ across the SQUID arising from the 50 Ω coaxial line carrying the bias current pulses. Using the estimated value, $C_s = 20$ fF, and including the term $1/R_l$ in Eq. (14) to give

$$K(\omega) = (\Phi_0 / 2\pi) i\omega [\hat{Y}(\omega) + 2i\omega C_j + 1/R_l], \qquad (19)$$

we obtain a good fit to our data with $R_l = 52\ \Omega$, which agrees well with the known cable impedance; we shall refer to this scenario, with small C_s and small R_l as case B. This fit, and fits for other values of Φ_S, are shown in Fig. 7.

To quantify the effect of RC-shunts on a SQUID when R_l is included, we note that a calculation for a SQUID with identical parameters, including R_l but with no RC-shunts, yields $T^* = 222$ mK for $\Phi_S = 0.01\Phi_0$ and a saturated 90% switching width of $\delta I_s^{90\%}/I_s^{50\%} = 0.0149$.

The damping effects of the SQUID bias leads led us to include on-chip series resistors in subsequent designs. We fabricated similar SQUIDs using 250 Ω on-chip resistors in series with the bias lines and with no RC-shunts. Using the theory developed in this paper, we fitted the low-temperature switching widths for one such device to obtain an effective lead impedance $R_l = 234\ \Omega$, which can be compared to the expected value of 300 Ω when the 50 Ω line impedance is included. Through separate experiments,[22] we verified that the power dissipated in this series resistance during the bias current pulses does not lead to appreciable heating.[23]
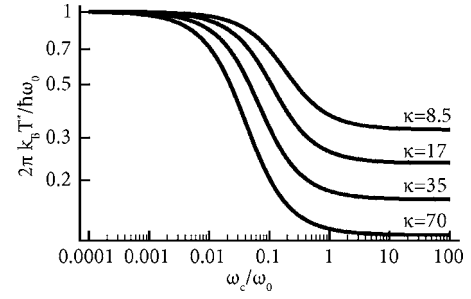
FIG. 8. Suppression of T^* for RC-shunted SQUID $2\pi k_B T^*/\hbar\omega_0$ vs ω_c/ω_0. Four curves are shown for different values of $\kappa \equiv C_s/C_j$.

IV. CALCULATIONS OF DECOHERENCE DUE TO RC-SHUNTS

In order for the enhanced sensitivity of the RC-shunted SQUID to be useful for measuring a flux qubit, it is important that the shunts not couple excessive dissipation to the qubit and thus limit decoherence times. In this section, we calculate the decoherence due to a SQUID with arbitrary shunt admittances (Fig. 1). The calculations are performed for a single-junction qubit for definiteness, but the results hold for any flux qubit, including three-junction qubits. In contrast to previous calculations,[8] we include the self-inductance of the SQUID loop, and the junctions are shunted individually.

In the spin-boson model, decoherence times are obtained from the environmental spectral density function $J(\omega)$, which can be found from the classical friction the phase of the qubit experiences from its environment.[16,24] For a total qubit flux Φ_Q^t and qubit potential $U_Q(\Phi_Q^t)$, one finds $J(\omega) = [(L_Q J_Q)^2 / 2\pi\hbar] \text{Im}[D(\omega)]$, where $D(\omega)$ is the linear coefficient in the Fourier-transformed equation of motion

$$D(\omega)\Phi_Q^t = -\partial U_Q / \partial \Phi_Q^t \qquad (20)$$

with the environmental coordinates eliminated.

We now model the decoherence induced when the SQUID is in its "off" state, that is, for zero bias current, using this formalism. To do this we must find the classical equation of motion for the qubit, including influences from the SQUID. We begin by splitting the total fluxes through the SQUID and the qubit into external and screening fluxes, $\Phi_S^t = \Phi_S + \Phi_S^s$ and $\Phi_Q^t = \Phi_Q + \Phi_Q^s$, respectively, where Φ_S and Φ_Q are fluxes from external sources. The screening fluxes arise from circulating currents in the SQUID (J_S) and qubit (J_Q), as

$$\begin{pmatrix} \Phi_Q^s \\ \Phi_S^s \end{pmatrix} = \begin{pmatrix} L_Q & M_{QS} \\ M_{QS} & L_S \end{pmatrix} \begin{pmatrix} J_Q \\ J_S \end{pmatrix}, \qquad (21)$$

where L_Q is the inductance of the qubit which has mutual inductance M_{QS} to the SQUID with self-inductance L_S. Equation (21) allows us to express the fluxes through currents by matrix inversion,

$$\begin{pmatrix} J_Q \\ J_S \end{pmatrix} = \frac{1}{M_\Sigma^2} \begin{pmatrix} L_S & -M_{QS} \\ -M_{QS} & L_Q \end{pmatrix} \begin{pmatrix} \Phi_Q^s \\ \Phi_S^s \end{pmatrix}, \qquad (22)$$

where $M_\Sigma^2 = L_Q L_S - M_{QS}^2 \geq 0$.

We can write current conservation at a node in the SQUID loop as $J_S = I_C + I_j + I_Y$, where the terms on the right are the current through the junction capacitance, junction inductance, and shunt admittance, respectively. Proceeding term by term, we have

$$I_C = C_j \dot{V}_i = (C_j \Phi_0 / 2\pi) \ddot{\gamma}_i, \qquad (23)$$

where we have introduced the junction voltages V_i and used dots to denote time derivatives. For $I_b = 0$, the symmetry of the two junctions is unbroken, so that Eq. (10) implies

$$\gamma_1 = -\gamma_2 = (\pi/\Phi_0)(\Phi_S^s + \Phi_S). \qquad (24)$$

Thus, we have $I_C = (C_j/2)\ddot{\Phi}_S^s$. The next term is given simply by the Josephson current-phase relation, $I_j = I_0 \sin \gamma_i$. Finally, the current through the shunt is simply $I_Y = V_i Y$. Thus, the equation of motion for the SQUID can be written as

$$(C_j/2)\ddot{\Phi}_S^s + I_0 \sin[\pi(\Phi_S + \Phi_S^s)/\Phi_0] + (Y/2)\dot{\Phi}_S^s$$
$$= (L_Q \Phi_S^s - M_{QS}\Phi_Q^s)/M_\Sigma^2. \qquad (25)$$

We expand the sine term for small Φ_S^s/Φ_0 and Fourier transform to obtain

$$\left[-\omega^2 \frac{C_j}{2} + i\omega \frac{Y(\omega)}{2} + \frac{L_Q}{M_\Sigma^2} + \frac{\pi I_0}{\Phi_0} \cos\left(\frac{\pi\Phi_S}{\Phi_0}\right) \right] \Phi_S^s$$
$$= -I_0 \sin(\pi\Phi_S/\Phi_0) - (M_{QS}/M_\Sigma^2)\Phi_Q^s. \qquad (26)$$

We henceforth simplify the notation by introducing the effective inductance of the SQUID L_{eff}, where $1/L_{\text{eff}} = L_Q/M_\Sigma^2 + (\pi I_0/\Phi_0)\cos(\pi\Phi_S/\Phi_0)$.

We perform a similar analysis for the qubit, in which current conservation yields

$$C_Q \ddot{\Phi}_Q^s + J_Q \sin[2\pi(\Phi_Q + \Phi_Q^s)/\Phi_0] = (L_S \Phi_Q^s - M_{QS}\Phi_S^s)/M_\Sigma^2. \qquad (27)$$

We do *not* linearize the Josephson term here, but instead include it in U_Q in Eq. (20). We now Fourier transform, regroup terms, and substitute Φ_S^s from Eq. (26) into Eq. (27) to find the Fourier-transformed equation of motion for the qubit in the form prescribed by Eq. (20), giving

$$D(\omega) = (L_S/M_\Sigma^2) - \omega^2 C_Q + (M_{QS}^2/M_\Sigma^4)$$
$$\times [(\omega^2 C_j - i\omega Y(\omega)/2) - (1/L_{\text{eff}})]^{-1}. \qquad (28)$$

Using $M_\Sigma^2 \simeq L_Q L_S$, we can write

$$J(\omega) = (J_Q^2 M_{QS}^2 / 2\pi\hbar L_S^2) \text{Im}\{ [(\omega^2 C_j - i\omega Y(\omega)/2) - (1/L_{\text{eff}})]^{-1} \}. \qquad (29)$$

This is the central result of this section.

We now consider the specific case of a purely resistive shunt, $Y = 1/R_s$, for which Eq. (29) becomes

$$J(\omega) = \frac{\alpha}{4} \left[\left(1 - \omega^2 C_j \frac{L_{\text{eff}}}{2}\right)^2 + \frac{\omega^2 L_{\text{eff}}^2}{R_s^2} \right]^{-1}. \qquad (30)$$

This expression is ohmic at low frequencies with $\alpha \equiv \lim_{\omega\to 0} 4J(\omega)/\omega = J_Q^2 M_{QS}^2 L_{\text{eff}}^2 / \pi\hbar L_S^2 R_s$. The internal effective LC-resonance of the SQUID appears as a high-
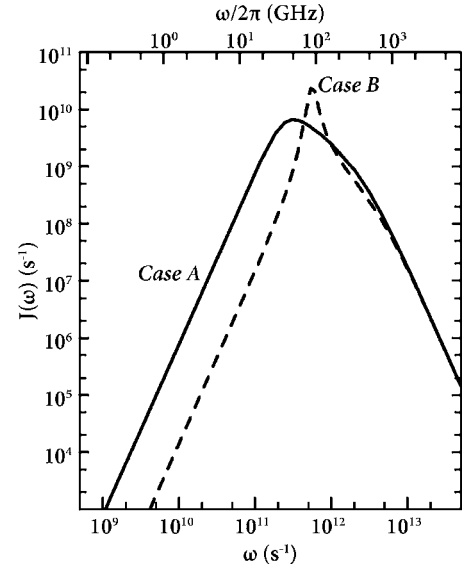
FIG. 9. $J(\omega)$ for a flux qubit coupled to an RC-shunted SQUID with parameters given in text. Solid line corresponds to case A and dashed line corresponds to case B.

frequency peak in $J(\omega)$, which may be broadened by the damping.

For the case of the RC-shunt, we substitute $Y(\omega) = \omega C_s \omega_c / (\omega - i\omega_c)$ into Eq. (29) to find

$$J(\omega) = (\alpha\omega^3/\omega_c^2)[4(\omega^2 L_{\text{eff}} C_{\text{eff}} - 1)^2$$
$$+ (\omega^2/\omega_c^2)(\omega^2 C_j L_{\text{eff}} - 2)^2]^{-1}, \qquad (31)$$

with effective capacitance $C_{\text{eff}} = C_j/2 + C_s/2$. Since $J(\omega)$ scales as ω^3, it is superohmic at low frequencies; at higher frequencies it contains a modified version of the LC-resonance peak of the SQUID. This expression is valid for a symmetric SQUID with zero current bias, where to first order the internal circulating current mode is decoupled from external impedance sources.[8] To account for the effect of R_l away from this special point, one must numerically solve the equations governing the coupling of the SQUID circulating current to external decoherence.[26]

To estimate the contribution of an RC-shunted SQUID to decoherence, we consider a symmetric SQUID with the escape widths of our measured device coupled to a hypothetical flux qubit with M_{QS} chosen to yield single-shot resolution at the 99% level: $L_S = 500$ pH, $I_0 = 1.96$ μA, $C_j = 9.3$ fF, $R_s = 40$ Ω, $L_Q = 200$ pH, $M_{QS} = 96$ pH, and $J_Q = 0.3$ μA. We will consider both case A, with $C_s = 153$ fF and $R_l = \infty$, and case B, with $C_s = 20$ fF and $R_l = 52$ Ω, as described in Sec. III both at a flux bias of $\Phi_S = \Phi_0/4$, where the SQUID resolution is near optimal [Fig. 6(c)], and with $I_b = 0$ so that Eq. (31) is valid. These parameters correspond to plasma frequencies in the SQUID junctions of 80 and 120 GHz and roll-off frequencies $\omega_c/2\pi = 26$ and 200 GHz, for cases A and B, respectively. We assume arbitrarily that the qubit has a tunneling frequency $\Delta/h = 1$ GHz. The behavior of $J(\omega)$ calculated from Eq. (31) is shown in Fig. 9. We see that $J(\omega)$ exhibits the LC-resonance of the SQUID near 51 GHz for case A and
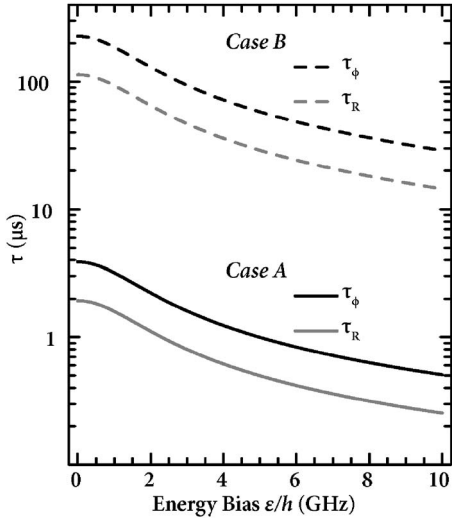
FIG. 10. Dephasing (τ_ϕ, black) and relaxation (τ_R, gray) times for flux qubit coupled to RC-shunted SQUID. Solid lines correspond to case A and dashed lines correspond to case B.

89 GHz for case B, while at the frequencies near 1 GHz relevant to the qubit it is well within the ω^3 regime for both cases.

Finally, we use $J(\omega)$ to calculate relaxation (τ_R^{-1}) and dephasing (τ_ϕ^{-1}) rates[25] for our qubit due to the RC-shunts:

$$\tau_R^{-1} = 4\pi(\Delta/\nu)^2 J(2\pi\nu)\coth(h\nu/2k_BT) \qquad (32)$$

and

$$\tau_\phi^{-1} = \tau_R^{-1}/2 + 2\pi\alpha(\epsilon/\nu)^2(k_BT/\hbar). \qquad (33)$$

Here, $\nu=(\Delta^2+\epsilon^2)^{1/2}$ is the qubit frequency, where ϵ is the bias of the qubit relative to the degeneracy point. For the RC-shunted SQUID, α vanishes because of the ω^3 dependence at low frequencies, so that $\tau_\phi=2\tau_R$. In Fig. 10 we plot τ_R and τ_ϕ versus ϵ. At $\epsilon=0$, $\tau_R=1.9$ μs and $\tau_\phi=3.9$ μs for case A, while for case B $\tau_R=113$ μs and $\tau_\phi=226$ μs; both times decrease with increasing ϵ for both cases because of the ω^3 dependence of α. For low ϵ, τ_ϕ is much longer than values currently observed in flux qubits without echoes, so that the readout device does not contribute significantly to dephasing. Hence, the RC-shunted SQUID achieves single-shot readout while inducing negligible decoherence in the qubit. By contrast, a readout SQUID with the same parameters except for purely resistive shunts of $R_s=40$ Ω would cause dephasing in 5.7 ns.

In this analysis we have assumed complete symmetry of the SQUID. We note that for a symmetric SQUID with zero bias current, noise currents generated by R_l decouple from the qubit to linear order;[8] however, even small asymmetries can cause the qubit to couple strongly to R_l, rapidly degrading its coherence, even for zero bias current. For example, borrowing the techniques developed in Ref. 26, we estimate that a 5% asymmetry in the critical current of the SQUID junctions would reduce τ_ϕ from 226 μs to approximately 1 μs at the degeneracy point for case B with $I_b=0$. However, it should be possible to compensate for this asymmetry by adjusting I_b.[27]

V. CONCLUSION

The need to resolve the state of a flux qubit in a single measurement while maintaining a weak coupling between the qubit and SQUID drives the development of techniques to enhance the sensitivity of the SQUID without a concomitant increase in the decoherence induced in the qubit. This requirement has led us to calculate the escape widths for a SQUID with an arbitrary, frequency-dependent shunt admittance across each junction, and with an arbitrary magnetic flux bias, in both the thermal and quantum regimes. We find that an appropriately designed, series R_sC_s shunt suppresses the thermal-to-quantum crossover temperature T^*, leading to narrower escape widths at low temperatures.

We used this model to explain the temperature dependence of the escape width for a SQUID equipped with such shunts for several values of flux bias. This device showed a switching distribution at low temperature that was narrower than what one would expect from a corresponding unshunted SQUID, improving the resolution by a factor of nearly 3. However, for this model to explain the observed degree of narrowing required a shunt capacitance an order of magnitude larger than the *a priori* value estimated for the interdigitated capacitors we constructed. We explained this result by including the effect of the SQUID lead impedance on the switching process; a model employing the *a priori* value of shunt capacitance combined with a lead impedance close to 50 Ω gave good agreement with the experimental data.

We further calculated the decoherence induced in a flux qubit by a SQUID with arbitrary shunt admittances. As a numerical example, we modeled a system in which our measured R_sC_s-shunted SQUID, using the *a priori* value of shunt capacitance and including the lead impedance, is coupled to a hypothetical (but realistic) qubit with parameters chosen to yield single-shot readout. This combination of devices yielded a dephasing time that ranged from about 200 μs at the degeneracy point to 30 μs at an energy bias of 10 GHz. These times are orders of magnitude longer than those observed in flux qubits due to inhomogeneous broadening[2,6] and obtained recently by means of spin echoes.[27] However, we emphasize that these calculated results are for a symmetric SQUID; when an asymmetry in the SQUID junction critical currents is included, the dephasing times are likely to be substantially reduced. This decoherence can be mitigated by including sufficiently large resistors in series with the SQUID leads.

As is made clear in Fig. 9, one can suppress T^*, and thereby narrow the low-temperature escape widths, by reducing the shunt resistance R_s or increasing the shunt capacitance C_s, or by a combination of both. Furthermore, inspection of Eq. (31) shows that $J(\omega) \to 0$ as $R_s \to 0$, so that the decoherence due to the shunts vanishes in this limit. Thus, a design with a purely capacitive shunt across each junction is the natural solution to the problem of obtaining a narrow distribution.

*Present address: Department of Physics, Syracuse University, Syracuse, NY 13244-1130.

†Present address: Department of Quantum Electronics, Institute for Physical High Technology, Albert-Einstein-Str. 9, 07745 Jena, Germany.

[1] C. van der Wal, A. ter Haar, F. Wilhelm, R. Schouten, C. J. P. M. Harmans, T. Orlando, S. Lloyd, and J. E. Mooij, Science **290**, 773 (2000).

[2] I. Chiorescu, Y. Nakamura, C. Harmans, and J. Mooij, Science **299**, 1869 (2003).

[3] J. Friedman, V. Patel, W. Chen, S. Tolpygo, and J. Lukens, Nature (London) **46**, 43 (2000).

[4] E. Il'ichev, N. Oukhanski, A. Izmalkov, T. Wagner, M. Grajcar, H.-G. Meyer, A. Smirnov, A. Maassen van den Brink, M. H. S. Amin, and A. M. Zagoskin, Phys. Rev. Lett. **91**, 097906 (2003).

[5] S. Saito, M. Thorwart, H. Tanaka, M. Ueda, H. Nakano, K. Semba, and H. Takayanagi, Phys. Rev. Lett. **93**, 037001 (2004).

[6] B. L. T. Plourde, T. L. Robertson, P. A. Reichardt, T. Hime, S. Linzen, C. E. Wu, and J. Clarke, cond-mat/0501679 (unpublished).

[7] R. Kleiner, D. Koelle, F. Ludwig, and J. Clarke, Proc. IEEE **92**, 1534 (2004).

[8] C. H. van der Wal, F. K. Wilhelm, C. J. P. M. Harmans, and J. E. Mooij, Eur. Phys. J. B **31**, 111 (2003).

[9] I. Affleck, Phys. Rev. Lett. **46**, 388 (1981).

[10] V. Lefevre-Seguin, E. Turlot, C. Urbina, D. Esteve, and M. H. Devoret, Phys. Rev. B **46**, 5507 (1992).

[11] B. L. T. Plourde, J. Zhang, K. B. Whaley, F. K. Wilhelm, T. L. Robertson, T. Hime, S. Linzen, P. A. Reichardt, C.-E. Wu, and J. Clarke, Phys. Rev. B **70**, 140501(R) (2004).

[12] U. Weiss, *Quantum Dissipative Systems*, in Series in Modern Condensed Matter Physics, 2nd ed., No. 10 (World Scientific, Singapore, 1999).

[13] J. M. Martinis, M. H. Devoret, and J. Clarke, Phys. Rev. B **35**, 4682 (1987).

[14] S.-X. Li, Y. Yu, Y. Zhang, W. Qiu, S. Han, and Z. Wang, Phys. Rev. Lett. **89**, 098301 (2002).

[15] F. Balestro, J. Claudon, J. P. Pekola, and O. Buisson, Phys. Rev. Lett. **91**, 158301 (2003).

[16] A. J. Leggett, Phys. Rev. B **30**, 1208 (1984).

[17] P. Joyez, D. Vion, M. Götz, M. H. Devoret, and D. Esteve, J. Supercond. **12**, 757 (1999).

[18] F. Portier, Ph.D. thesis, CEA Saclay, 2002.

[19] D. Esteve (private communication).

[20] B. Chesca, R. Schulz, B. Goetz, C. Schneider, H. Hilgenkamp, and J. Mannhart, Phys. Rev. Lett. **88**, 177003 (2002).

[21] G. Cardano, *Ars Magna* (1545).

[22] P. A. Reichardt, T. Hime, S. Linzen, B. L. T. Plourde, T. L. Robertson, C. E. Wu, J. Clarke, and F. K. Wilhelm, Bull. Am. Phys. Soc. **49**, A37.004 (2004).

[23] F. C. Wellstood, C. Urbina, and J. Clarke, Phys. Rev. B **49**, 5942 (1994).

[24] F. K. Wilhelm, M. J. Storcz, C. H. van der Wal, C. J. P. M. Harmans, and J. E. Mooij, Adv. Solid State Phys. **43**, 763 (2003).

[25] Y. Makhlin, G. Schön, and A. Shnirman, Rev. Mod. Phys. **73**, 357 (2001).

[26] C. H. van der Wal, Ph.D. thesis, Delft University of Technology, 2001.

[27] P. Bertet, I. Chiorescu, G. Burkard, K. Semba, C. J. P. M. Harmans, D. DiVincenzo, and J. E. Mooij, cond-mat/0412485 (unpublished).